OPEN ACCESS

KING'S College LONDON

King's Research Portal

DOI:
10.1364/OPTICA.5.001502

Document Version
Publisher's PDF, also known as Version of record

Link to publication record in King's Research Portal

Citation for published version (APA):
Wells, B., Bykov, A. Y., Marino, G., Nasir, M. E., Zayats, A. V., & Podolskiy, V. A. (2018). Structural second-order nonlinearity in plasmonic metamaterials. *Optica*, *5*(12), 1502-1507. https://doi.org/10.1364/OPTICA.5.001502

Citing this paper
Please note that where the full-text provided on King's Research Portal is the Author Accepted Manuscript or Post-Print version this may differ from the final Published version. If citing, it is advised that you check and use the publisher's definitive version for pagination, volume/issue, and date of publication details. And where the final published version is provided on the Research Portal, if citing you are again advised to check the publisher's website for any subsequent corrections.

General rights
Copyright and moral rights for the publications made accessible in the Research Portal are retained by the authors and/or other copyright owners and it is a condition of accessing publications that users recognize and abide by the legal requirements associated with these rights.

•Users may download and print one copy of any publication from the Research Portal for the purpose of private study or research.
•You may not further distribute the material or use it for any profit-making activity or commercial gain
•You may freely distribute the URL identifying the publication in the Research Portal

Take down policy
If you believe that this document breaches copyright please contact librarypure@kcl.ac.uk providing details, and we will remove access to the work immediately and investigate your claim.

Download date: 04. May. 2023

Research Article Vol. 5, No. 12 / December 2018 / Optica 1502

Structural second-order nonlinearity in plasmonic metamaterials

Brian Wells,[1,2,†] Anton Yu. Bykov,[3,†] Giuseppe Marino,[3,4,†] Mazhar E. Nasir,[3] Anatoly V. Zayats,[3,5] and Viktor A. Podolskiy[1,6]

[1]Department of Physics and Applied Physics, University of Massachusetts Lowell, Lowell, Massachusetts 01854, USA
[2]Department of Physics, University of Hartford, Hartford, Connecticut 06117, USA
[3]Department of Physics and London Centre for Nanotechnology, King's College London, London WC2R 2LS, UK
[4]Matériaux et Phénoménes Quantiques, Université Paris Diderot-CNRS, F-75013 Paris, France
[5]e-mail: anatoly.zayats@kcl.ac.uk
[6]e-mail: viktor_podolskiy@uml.edu

Received 13 July 2018; revised 24 September 2018; accepted 2 October 2018 (Doc. ID 338796); published 26 November 2018

Nonlinear processes are at the core of many optical technologies whose further development require optimized materials suitable for nanoscale integration. Here we demonstrate the emergence of a strong bulk second-order nonlinear response in a plasmonic nanorod composite comprised of centrosymmetric materials. We develop an effective-medium description of the underlying physics, compare its predictions to the experimental results, and analyze the limits of its applicability. We demonstrate strong *tunable* generation of the *p*-polarized second-harmonic light in response to either *s*- or *p*-polarized excitation. High second-harmonic enhancement is observed for fundamental frequencies in the epsilon-near-zero spectral range. The work demonstrates emergence of structurally tunable nonlinear optical response in plasmonic composites and presents a new nonlinear optical platform suitable for integrated nonlinear photonics. © 2018 Optical Society of America under the terms of the OSA Open Access Publishing Agreement

https://doi.org/10.1364/OPTICA.5.001502

1. INTRODUCTION

Second-harmonic generation (SHG), a phenomenon in which the incoming radiation of a frequency ω is converted into the signal at a double frequency 2ω, is a fundamental nonlinear optical process that enables high-resolution microscopy, laser technology, and surface studies [1–5]. Materials with strong second-order nonlinear response can further advance a broad class of photonic applications, including frequency conversion, optical information processing, sensing, security, and healthcare. Unfortunately, natural optical materials with strong second-order nonlinearity are few, and new solutions are needed to develop nonlinear optics in compact, wavelength-scale, and integrated systems.

Recent advances in nano- and microfabrication have brought into play a new class of composite media, often called metamaterials, whose optical properties are determined by shape and mutual arrangement of their components [6–10]. Metamaterials provide a flexible platform for engineering linear optical behavior that can range from isotropic [6,9] to anisotropic and hyperbolic [11,12] to chiral and bianisotropic [10]. As a rule, linear optical response of metamaterials can be related to averaged linear optical response of their components via the effective-medium theory (EMT) [9,10]. Similarly, the effective nonlinear susceptibility of the composite can be related to the nonlinear susceptibilities of constituent materials [13–16]. Recently, nonlinear metamaterials have been used for engineering third-order (Kerr-type) nonlinearity, achieving on-demand spectral response, including its sign and polarization control [17–21].

In this work, we show that re-shaping of electromagnetic fields in metamaterials with plasmonic components can be used to transform SHG from surface- to volume-dominated regime and engineer strong tunable bulk nonlinear response in plasmonic composites. We experimentally demonstrate tunable SHG from plasmonic nanorod metamaterials, develop a theoretical description of the observed phenomena, and prove that the nonlinear response can be engineered by changing structural parameters of the composite.

2. FABRICATION AND LINEAR OPTICAL RESPONSE

We consider SH response of the metamaterial comprising an array of gold nanorods in an alumina matrix [Fig. 1(a)]. When the nanorod radius r and inter-rod separation a are much smaller than the operating wavelength λ, such metamaterial behaves as a uniaxial crystal with an optical axis parallel to the nanorods [11,22,23].

The linear optical response of the metamaterial is described by a diagonal permittivity tensor $\hat{\epsilon}$ with components $\epsilon_{xx} = \epsilon_{yy} = \epsilon_{\perp}$ and $\epsilon_{zz} \neq \epsilon_{\perp}$. If the material absorption is not too small and $r \ll a \ll \lambda$, the effective-medium parameters can be related to the relative permittivity of the host ϵ_h and nanorod ϵ_{Au} materials, and the nanorod concentration $p = \pi r^2/a^2$ via

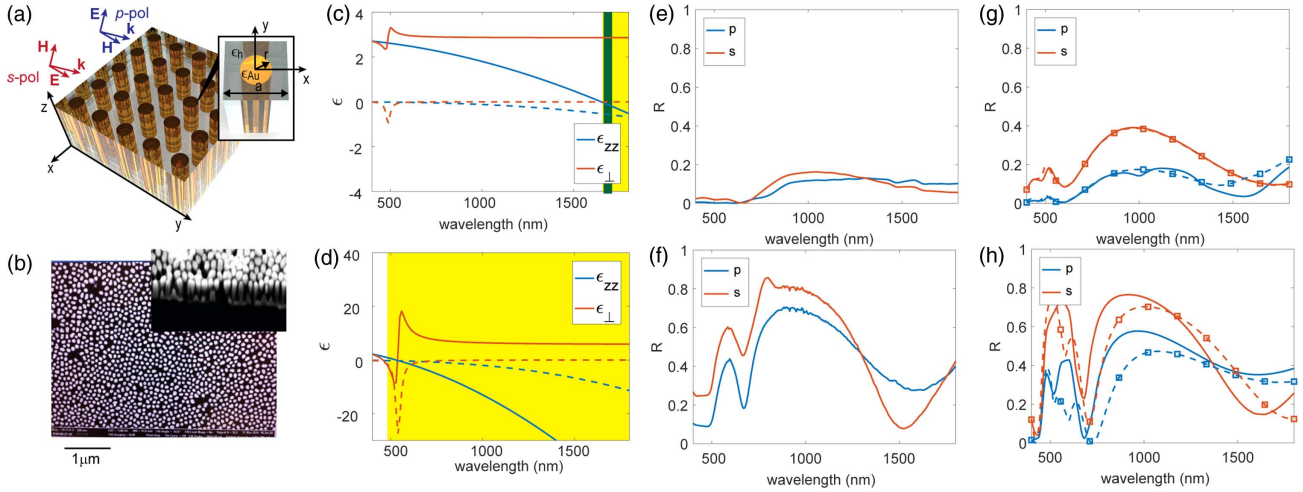

Fig. 1. (a) Schematic geometry of a metamaterial along with orientation of the fields and wavevectors considered in modeling and experiments. (b) SEM image of the nanorods after removal of the AAO matrix. (c), (d) Real (solid lines) and imaginary (dashed lines) parts of the effective permittivity of samples A (c) and B (d); green and yellow areas highlight the spectral ranges of the ENZ behavior for sample A and hyperbolic dispersion for both samples, repectively. (e)–(h) Linear reflection spectra for metamaterials A (e), (g) and B (f), (h): experiment (e), (f) and theoretical modeling (g), (h) using the full-wave finite-element simulations (solid lines) and the effective-medium theory (dashed lines). Angle of incidence in all figures is fixed at 45°.

$$\epsilon_\perp = \epsilon_h \frac{(1+p)\epsilon_{\mathrm{Au}} + (1-p)\epsilon_h}{(1+p)\epsilon_h + (1-p)\epsilon_{\mathrm{Au}}}, \quad \epsilon_{zz} = p\epsilon_{\mathrm{Au}} + (1-p)\epsilon_h. \quad (1)$$

In the limit of small absorption, long nanorods, or large unit cells, the deviations from the local EMT predictions can be quantitatively explained by incorporating retardation effects into nonlocal (wavevector-dependent) EMT [24–27].

Importantly, components of the effective permittivity tensor $\epsilon_\perp$ and ϵ_{zz} can be of different signs (Fig. 1), tuning the nanorod composite between anisotropic dielectric, epsilon near zero (ENZ) media, and a unique "hyperbolic metamaterial," which enables propagation of waveguided modes with subwavelength light confinement that in turn enhance light–matter interactions in the metamaterial [10,12,23,28].

Plasmonic nanorod metamaterials were fabricated via Au electrodeposition into nanoporous anodized aluminum oxide (AAO) templates on a glass substrate [29]. An Al film of 500 nm thickness was deposited on a substrate by magnetron sputtering. The substrate comprises a glass cover slip with a 10-nm-thick adhesive layer of tantalum pentoxide and a 7-nm-thick Au film acting as a weakly conducting layer. Highly ordered, nanoporous AAO was synthesized by a two-step anodization in 0.3M oxalic and 0.3M selenic acid at 40 V and 48 V, respectively. Gold electrodeposition was performed with a three-electrode system using a non-cyanide solution. The length of nanorods was controlled by the electrodeposition time. Fabricated metamaterials were ion-milled to smooth the top surface and ensure that the nanorods are of the same length [30]. We estimate that the variation of the nanorod height is on a few nm level, so that optical properties of the composites are not affected by surface roughness. In particular, SHG, which is very sensitive to surface roughness, exhibited neither an appreciable diffuse component nor unpolarized signal, which typically appear for rough surfaces. The samples were annealed at 300°C to improve Au optical properties.

Two samples were used in this study: sample A composed of 18-nm-diameter, 220-nm-long nanorods arranged in 110-nm period array, and sample B comprising 67-nm-diameter, 150-nm-long nanorods in the array of 100-nm period. Reflectivity and the effective-medium parameters of both samples are presented in Fig. 1. Sample A exhibits the effective plasma frequency at around $\lambda_0 \simeq 1500$ nm, while sample B operates in hyperbolic regime throughout visible and infrared spectral ranges. The linear reflection spectra of the composites are typical of anisotropic metamaterials, showing resonances due to the Fabry–Perot modes of the metamaterial slab [23,28]. The measured spectra correspond well to the numerical models for both the full-wave solutions of the Maxwell's equations using finite-element method (FEM) [31] and the transfer matrix formalism that approximates metamaterials as homogeneous layers with anisotropic permittivity given by Eq. (1).

Slight disagreement between the experiment and numerical calculations in the visible range is due to the interband transitions in gold that are not well described by the Drude model, $\epsilon_{\mathrm{Au}} = \epsilon_b - \omega_p^2/[\omega(\omega - i\tau)]$ with plasma frequency $\omega_p = (e^2 n_0/m_e\epsilon_0)^{1/2} = 1.36\times10^{16}\ \mathrm{s}^{-1}$, inelastic scattering frequency $\tau = 2.1\times10^{14}\ \mathrm{s}^{-1}$, parameter $\epsilon_b = 9.5$, and ϵ_0, e, m_e, and n_0 being the permittivity of free space, electron charge, electron mass, and free-electron density in gold, respectively [32].

3. NONLINEAR OPTICAL RESPONSE

SHG spectroscopy was performed using light from the optical parametric amplifier (200 fs pulse trains at the repetition rate of 200 kHz and average power up to 50 mW in near-IR wavelength range 1100–1800 nm). The laser light polarization was controlled to achieve *p*- or *s*-polarized fundamental light incident on the sample at an angle of incidence of 45° with a spot approximately 30–50 μm in diameter. The reflected *p*- or *s*- polarized SH light was spectrally selected using the set of short-pass optical filters and measured with the spectrometer and the cooled charged-coupled device (CCD) camera. In order to compensate for pulse energy and pulse duration fluctuations, the measured signal was normalized to a reference SHG measured in reflection from *β*-barium borate (BBO) crystal. Also, the SHG from each sample

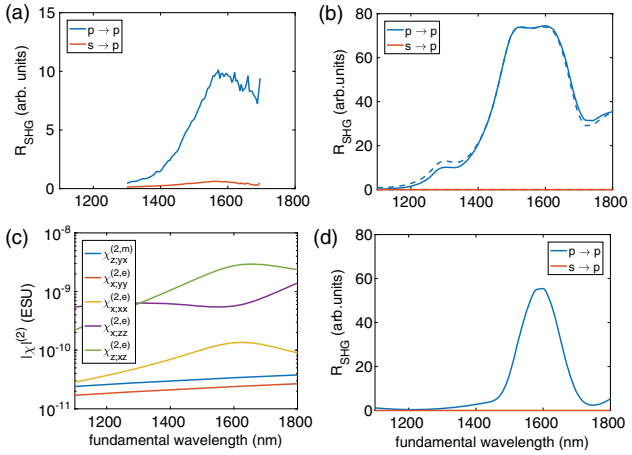

Fig. 2. SHG spectra for different polarization configurations from metamaterial A at an angle of incidence of 45°: (a) experimental spectra normalized with $s \rightarrow p$ SHG from z-quartz at $\lambda_0 = 1300$ nm; (b) spectra simulated using the full-wave numerical modeling with the nonlinear polarization described by Eq. (2) (solid lines) and by the simplified model Eq. (3) (dashed lines). (c) Spectral dependence of the non-vanishing components of the effective polarizability matrix. (d) SHG spectra simulated with the nonlinear EMT model [Eqs. (4) and (5)].

was compared to the signal from a z-quartz plate. As a result, the SHG data for samples A and B can be directly compared to each other.

SHG spectra of the two samples fundamentally differ from each other. Sample A exhibits strong *p*-polarized SHG emission in response to a *p*-polarized pump in the ENZ frequency range (Fig. 2). At the same time, SHG signal generated by sample B (Fig. 3) exhibits pronounced maxima associated with excitation of the metamaterial slab modes [28] for both *p*- and *s*-polarized excitation. Interestingly, the SHG intensity from sample B under *s*-polarized excitation is approximately four times stronger than under *p*-polarized pump, indicating the important role of local fields inside the metamaterial, as was observed previously for the nanoparticle composites [33].

The spectral and polarization dependences of the SHG are in a good agreement with the full-wave numerical simulations (Figs. 2 and 3) that implement the hydrodynamic model of the SHG in plasmonic media [28,34,35] (see Supplement 1) with the nonlinear polarization of gold given by

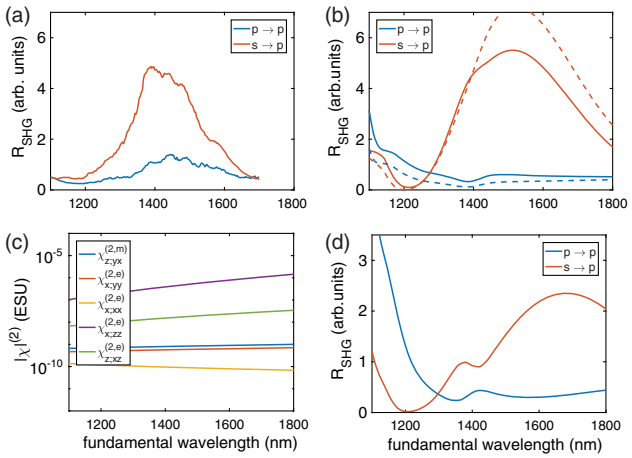

Fig. 3. Same as Fig. 2 but for sample B.

$$\mathbf{P}_{2\omega} = \frac{1}{2\omega(2\omega - i\tau)}\left\{\sum_{\alpha}\frac{\partial}{\partial r_\alpha}\left(\frac{\mathbf{j}_\omega j_{\omega;\alpha}}{en_0}\right) - \frac{e}{m_e}[\epsilon_0(\nabla\cdot\mathbf{E}_\omega)\mathbf{E}_\omega + \mathbf{j}_\omega \times \mathbf{B}_\omega]\right\}, \quad (2)$$

where ω and 2ω represent the fundamental and SH frequencies, respectively, index α represents the Cartesian coordinates, and $\mathbf{E}, \mathbf{B}, \mathbf{j}$ are the electric field, magnetic induction, and current density, respectively (the quantitative difference between numerical and experimental results for sample A can be explained by deviation of optical absorption of solution-derived gold from the Drude model used in this work [36]).

The detailed analysis shows that SHG efficiency and polarization dependencies are complex functions of the effective medium parameters, thickness of the metamaterial slab, and angle of illumination θ [28]. Nevertheless, in all cases, the nonlinear polarization, and, therefore, SHG, is dominated by the terms related to the components of the electromagnetic fields that have nonvanishing unit-cell averages [37] and to $\partial/\partial z$ derivatives of these components. These terms depend on polarization of the incident beam and are given by

$$P^{(p)}_{2\omega;x} = -\frac{1}{2\omega(2\omega - i\tau)}\left(\frac{e}{m}j_{\omega;z}B_{\omega;y} + \frac{1}{ne}\left[j_{\omega;z}\frac{\partial j_{\omega;x}}{\partial z} - j_{\omega;x}\frac{\partial j_{\omega;z}}{\partial z}\right]\right),$$

$$P^{(s)}_{2\omega;x} = \frac{1}{2\omega(2\omega - i\tau)}\frac{e}{m}j_{\omega;y}B_{\omega;z},$$

$$P^{(p)}_{2\omega;z} = \frac{1}{2\omega(2\omega - i\tau)}\left(\frac{e}{m}j_{\omega;x}B_{\omega;y} - \frac{2j_{\omega;z}}{ne}\frac{\partial j_{\omega;z}}{\partial z}\right),$$

$$P^{(s)}_{2\omega;z} = -\frac{1}{2\omega(2\omega - i\tau)}\frac{e}{m}j_{\omega;y}B_{\omega;x}. \quad (3)$$

This is illustrated in Figs. 2(b) and 3(b), which compare SHG predictions according to simplified Eq. (3) and full-wave solutions [Eq. (2)]. It is seen that Eq. (3) largely agrees with the full-wave solutions of the Maxwell's equations, while slightly overestimating the reflected SHG of sample B. At the same time, Eq. (3) underestimates the transmitted SHG for this sample (see Supplement 1), so that the total SHG predicted by the simplified model is in line with predictions of the full-wave calculations. Note that the simplified model predicts $P_{2\omega;y} = 0$, resulting in only *p*-polarized SHG signal, in line with the experiment as well as with the predictions of the full-wave calculations.

Using Eqs. (3) and the constituent relationship $\mathbf{j} = i\omega\epsilon_0\epsilon_{\mathrm{Au}}\mathbf{E}$, it becomes possible to represent the unit-cell-averaged nonlinear polarization in the metamaterial as a quadratic form of the (unit-cell-averaged) fields, introducing the effective *bulk* second-order nonlinear susceptibilities $\chi^{(2,e)}$ and $\chi^{(2,m)}$:

$$P_{2\omega;\alpha} = \sum_{\beta,\gamma}[\chi^{(2,e)}_{\alpha;\beta\gamma}E_{\omega;\beta}E_{\omega;\gamma} + \chi^{(2,m)}_{\alpha;\beta\gamma}E_{\omega;\beta}B_{\omega;\gamma}], \quad (4)$$

where the Greek subscripts represent the Cartesian coordinates x, y, and z.

Components of the effective nonlinear susceptibility were calculated in the limit of the validity of local EMT [Eq. (1)], which yields homogeneous fields across the cross section of the nanorods [10,24, and Supplement 1], by substituting explicit relationships between field components inside the nanorod, their unit-cell averages, frequency, and components of the wavevector, resulting in

$$\chi^{(2,e)}_{x;xx} = N^p L \epsilon_{\mathrm{Au}} k_x \frac{\epsilon_\perp}{\epsilon_{zz}},$$
$$\chi^{(2,e)}_{x;zz} = N^p \left(\frac{p\epsilon_{zz}\omega_p^2 + \epsilon_{zz}\epsilon_{\mathrm{Au}} L\omega^2}{k_x c^2} - \epsilon_{\mathrm{Au}} L k_x \right),$$
$$\chi^{(2,e)}_{z;xz} = -N^p/2 \left(L \frac{\omega_p^2 \epsilon_{zz}}{c^2 k_x} - 2pk_x \epsilon_{\mathrm{Au}} \frac{\epsilon_\perp}{\epsilon_{zz}} \right),$$
$$\chi^{(2,m)}_{z;yx} = -2L\epsilon_0 \epsilon_{\mathrm{Au}} \frac{e}{m} \frac{\omega^2}{\omega_p^2} [\epsilon_{\mathrm{Au}}(2\omega) - \epsilon_b],$$
$$\chi^{(2,e)}_{x;yy} = -\chi^{(2,m)}_{z;yx} \frac{k_x}{\omega}. \quad (5)$$

Here, $N^p = 2\epsilon_0 \epsilon_{\mathrm{Au}} (e/m)(\omega^3/\omega_p^4)(\epsilon_{\mathrm{Au}}(2\omega) - \epsilon_b)$ is the normalization parameter, $k_x = \omega \sin\theta/c$ is the transverse component of the wavevector, and $L = 2p\epsilon_b/[\epsilon_{\mathrm{Au}}(\omega) + \epsilon_b]$ represents the relationship between the E_x and E_y components of the electric field in the nanorod and its unit-cell-averaged values. The first three components describe SHG excitation due to *p*-polarized fundamental light, while the latter two represent the SH generated by the *s*-polarized light.

4. DISCUSSION

Equations (4) and (5) represent the main result of this work: the metamaterial as a whole exhibits dipolar-like nonlinear response even though its material constituents lack bulk dipolar $\chi^{(2)}$. The effective nonlinear susceptibilities of plasmonic nanorod composite are determined primarily by the structure of the local fields inside it [37]. Components of the effective nonlinear susceptibility depend on an angle of incidence so that the symmetry of the metamaterial is broken by the internal fields, except at normal incidence when the electric-dipole SHG is forbidden due to symmetry considerations. The explicit dependence of the effective nonlinear susceptibility on the wavenumber reflects the *structural* origin of the nonlinearity of a metamaterial.

The developed nonlinear EMT adequately predicts both spatial distribution of nonlinear polarization (Supplement 1) and spectral SH response [Figs. 2(d) and 3(d)] with exception of a small red shift of the SHG spectra for sample B, which is related to the red shift in a linear reflectivity observed in Fig. 1. Calculated values of an effective nonlinear response of the composite $\chi^{(2)} \sim 10^{-10}$–10^{-6} [electrostatic units, ESU] [Figs. 2(c), 3(c), and 4] indicate relatively strong nonlinearity, which favorably compares to common nonlinear-optical crystals, including quartz, potassium dihydrogen phosphate (KDP) ($\chi^{(2)} \sim 10^{-9}$ ESU), and $LiNbO_3$ ($\chi^{(2)} \sim 10^{-7}$ ESU) [1,2]. Experimental data are in line with calculated values for the nonlinear susceptibility for both studied metamaterials. SHG intensity from the composites can be further optimized by manipulating geometry and reducing losses.

The main limitation on the effective-medium nonlinear description, presented in this work, comes from the granularity of metamaterial. In particular, the local EMT that underpins the final expressions in Eq. (1) assumes local behavior of the constituents, dipolar quasistatic field between the nanorods, and does not account for propagation of cylindrical plasmons along the nanorods. Nonlocal response of a free-electron plasma [23,38] may become relevant for composites with ultra-thin nanorods ($r \ll 1/k_F \sim \lambda_0/100$, with k_F being the Fermi wavenumber). Contributions of retardation effects and spatial dispersion may affect field distribution in the composites with a nanorod concentrations $p \gtrsim 0.3$. In the limit $r \ll \lambda$, these effects can be taken into account by including retardation effects [24] in the nonlocal Maxwell–Garnett formalism. Excitation of cylindrical plasmons primarily affects composites with low loss operating across elliptic and ENZ regimes. This limitation can be addressed by including propagation of additional electromagnetic waves (with linear response described in Ref. [25]) into the developed formalism. Nonlocal EMT can be further developed to incorporate non-quasistatic effects. Granularity of the composite must also be considered when emission of SH light is calculated. We expect that including the high-index "longitudinal" modes through nonlocal EMT [25,39] may further improve predictive power of the formalism presented in this work.

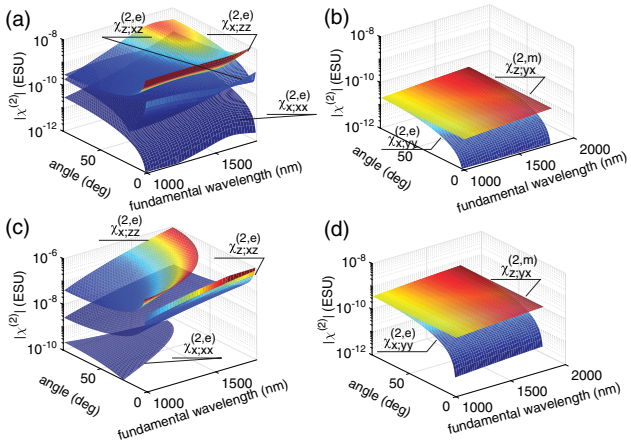

Fig. 4. Spectral and angular dependences of the components of the effective nonlinear polarizability for sample A (a), (b) and sample B (c), (d) for (a), (c) *p*- and (b), (d) *s*-polarized fundamental light.

In contrast to common nonlinear optical crystals with fixed optical properties, the structural origin of the second-order nonlinearity in metamaterials provides a platform for engineering not only spectral but also polarization properties of a nonlinear response. For example, the structural parameters of the nanorod metamaterials can be tuned to achieve dominant SHG contribution from either $p \to p$ (Fig. 2) or $s \to p$ (Fig. 3) polarization configurations [28,33].

In the former case, the metamaterial operates in the ENZ ($\epsilon_{zz} \simeq 0$) regime at a fundamental frequency $\lambda_0 \simeq 1600$ nm. The relatively weak effective nonlinear polarizability is compensated by the strong enhancement of *z* component of the electric field (a similar response has been predicted for bulk, nontunable, ENZ materials [20,40]). Interestingly, numerical calculations [Fig. 5(a)] suggest that material absorption in gold (which

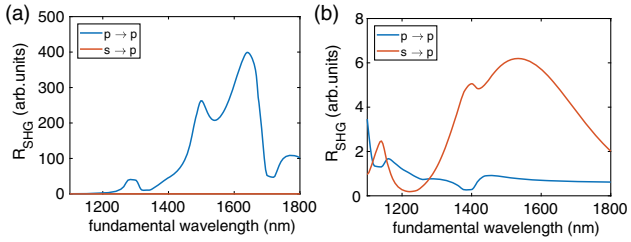

Fig. 5. Full-wave numerical modeling of the SHG spectra from low-loss analogs of sample A (a) and sample B (b). The loss is decreased by two times compared to Figs. 2(b) and 3(b).

effectively limits the value of $|\epsilon_{zz}|$) plays the role of the limiting factor in the SHG process in the ENZ regime. Reducing losses in the gold by a factor of 2 (achieved in calculations by reducing scattering frequency τ to the value that is in line with bulk Au $\tau = 1.05 \times 10^{-14}$ s [32]) has a potential to increase SHG efficiency in the metamaterial by an order of magnitude.

In another limit, the metamaterial operates in the hyperbolic regime so that the enhancement of the local field is attributed mainly to the Fabry–Perot modes of the metamaterial slab of a finite thickness [28]. This modest enhancement of a local field does not significantly depend on material absorption [Fig. 5(a)] and, being accompanied by a relatively strong nonlinear polarizability, once again results in a strong SH response of the metamaterial.

5. CONCLUSION

We have demonstrated the emergence of structural nonlinearity in composite metamaterials. The approach, presented here on the example of SHG from plasmonic nanorod metamaterials, can be extended to analyze nonlinear response of a broad class of composites, such as plasmonic nanoparticle metasurfaces [33] and metamaterials based on noncentrosymmetric, strongly nonlinear materials, such as AlGaAs nanopillars [41]. Structural nonlinearity opens the door to utilize composite media to engineer spectral and polarization nonlinear response beyond what is available with naturally occurring materials.

All the data supporting this research are presented in the article and in the supplementary material.

Funding. Army Research Office (ARO) (W911NF-12-1-0533, W911NF-16-1-0261); Engineering and Physical Sciences Research Council (EPSRC) (UK); H2020 European Research Council (ERC) iPLASMM project (321268); Royal Society; Wolfson Foundation.

See Supplement 1 for supporting content.

†These authors contributed equally to this work.

REFERENCES AND NOTES

1. R. W. Boyd, ed., *Nonlinear Optics*, 2nd ed. (Academic, 2003).
2. Y. Shen, *The Principles of Nonlinear Optics* (Wiley, 1984).
3. P. Campagnola and C.-Y. Dong, "Second harmonic generation microscopy: principles and applications to disease diagnosis," Laser Photon. Rev. **5**, 13–26 (2011).
4. M. Fiebig, V. V. Pavlov, and R. V. Pisarev, "Second-harmonic generation as a tool for studying electronic and magnetic structures of crystals: review," J. Opt. Soc. Am. B **22**, 96–118 (2005).
5. P. Segovia, G. Marino, A. V. Krasavin, N. Olivier, G. A. Wurtz, P. A. Belov, P. Ginzburg, and A. V. Zayats, "Hyperbolic metamaterial antenna for second-harmonic generation tomography," Opt. Express **23**, 30730–30738 (2015).
6. J. B. Pendry, "Negative refraction makes a perfect lens," Phys. Rev. Lett. **85**, 3966–3969 (2000).
7. N. Engheta, "Circuits with light at nanoscales: optical nanocircuits inspired by metamaterials," Science **317**, 1698–1702 (2007).
8. C. Kern, M. Kadic, and M. Wegener, "Experimental evidence for sign reversal of the hall coefficient in three-dimensional metamaterials," Phys. Rev. Lett. **118**, 016601 (2017).
9. G. W. Milton, *The Theory of Composites*, 1st ed. (Cambridge University, 2002).
10. M. A. Noginov and V. A. Podolskiy, eds., *Tutorials in Metamaterials* (CRC Press, 2012).
11. T. Dumelow and D. Tilley, "Optical properties of semiconductor superlattices in the far infrared," J. Opt. Soc. Am. A **10**, 633–645 (1993).
12. A. Poddubny, I. Iorsh, P. Belov, and Y. Kivshar, "Hyperbolic metamaterials," Nat. Photonics **7**, 948–957 (2013).
13. K. C. Rustagi and C. Flytzanis, "Optical nonlinearities in semiconductor-doped glasses," Opt. Lett. **9**, 344–346 (1984).
14. D. Stroud and P. M. Hui, "Nonlinear susceptibilities of granular matter," Phys. Rev. B **37**, 8719–8724 (1988).
15. D. J. Bergman, "Nonlinear behavior and 1/f noise near a conductivity threshold: effects of local microgeometry," Phys. Rev. B **39**, 4598–4609 (1989).
16. J. W. Haus, N. Kalyaniwalla, R. Inguva, M. Bloemer, and C. M. Bowden, "Nonlinear-optical properties of conductive spheroidal particle composites," J. Opt. Soc. Am. B **6**, 797–807 (1989).
17. M. Kauranen and A. Zayats, "Nonlinear plasmonics," Nat. Photonics **6**, 737–748 (2012).
18. N. N. Lepeshkin, A. Schweinsberg, G. Piredda, R. S. Bennink, and R. W. Boyd, "Enhanced nonlinear optical response of one-dimensional metal-dielectric photonic crystals," Phys. Rev. Lett. **93**, 123902 (2004).
19. A. Neira, N. Olivier, M. E. Nasir, W. Dickson, G. A. Wurtz, and A. V. Zayats, "Eliminating material constraints for nonlinearity with plasmonic metamaterials," Nat. Commun. **6**, 7757 (2015).
20. D. de Ceglia, S. Campione, M. A. Vincenti, F. Capolino, and M. Scalora, "Low-damping epsilon-near-zero slabs: nonlinear and nonlocal optical properties," Phys. Rev. B **87**, 155140 (2013).
21. L. Nicholls, F. J. Rodríguez-Fortuño, M. E. Nasir, R. M. Cordova-Castro, N. Olivier, G. A. Wurtz, and A. V. Zayats, "Ultrafast synthesis and switching of light polarization in nonlinear anisotropic metamaterials," Nat. Photonics **11**, 628–633 (2017).
22. R. Wangberg, J. Elser, E. E. Narimanov, and V. A. Podolskiy, "Nonmagnetic nanocomposites for optical and infrared negative-refractive-index media," J. Opt. Soc. Am. B **23**, 498–505 (2006).
23. N. Vasilantonakis, M. E. Nasir, W. Dickson, G. A. Wurtz, and A. V. Zayats, "Bulk plasmon-polaritons in hyperbolic nanorod metamaterial waveguides," Laser Photon. Rev. **9**, 345–353 (2015).
24. B. M. Wells, W. Guo, and V. A. Podolskiy, "Homogenization of nanowire-based composites with anisotropic unit-cell and layered substructure," MRS Commun. **6**, 23–29 (2016).
25. B. M. Wells, A. V. Zayats, and V. A. Podolskiy, "Nonlocal optics of plasmonic nanowire metamaterials," Phys. Rev. B **89**, 035111 (2014).
26. V. Agranovich and V. Kravtsov, "Notes on crystal optics of superlattices," Solid State Commun. **55**, 85–90 (1985).
27. Note that these nonlocal corrections originate from the composite nature of the plasmonic metamaterial and not from the optical response of its components, which is assumed to be described by local ϵ_{Au} and ϵ_h.
28. G. Marino, P. Segovia, A. V. Krasavin, P. Ginzburg, N. Olivier, G. A. Wurtz, and A. V. Zayats, "Second-harmonic generation from hyperbolic plasmonic nanorod metamaterial slab," Laser Photon. Rev. **12**, 1700189 (2018).
29. M. E. Nasir, S. Peruch, N. Vasilantonakis, W. P. Wardley, W. Dickson, G. A. Wurtz, and A. V. Zayats, "Tuning the effective plasma frequency of nanorod metamaterials from visible to telecom wavelengths," Appl. Phys. Lett. **107**, 121110 (2015).
30. A. V. Krasavin, M. E. Nasir, W. Dickson, and A. V. Zayats, "Reactive tunnel junctions in electrically-driven plasmonic nanorod metamaterials," Nat. Nanotechnol. **13**, 159–164 (2018).
31. The commercial software (COMSOL, www.comsol.com) implements a model of a periodic Au nanorod array with ϵ_{Au} given by Drude model, $\epsilon_{\mathrm{Al_2O_3}} \approx 2.74$, and geometrical parameters (r, a) deduced from the structures used in the experiments.
32. P. B. Johnson and R. W. Christy, "Optical constants of the noble metals," Phys. Rev. B **6**, 4370–4379 (1972).
33. T. Stefaniuk, N. Olivier, A. Belardini, C. P. T. McPolin, C. Sibilia, A. A. Wronkowska, A. Wronkowski, T. Szoplik, and A. V. Zayats, "Self-assembled silver-germanium nanolayer metamaterial with the enhanced nonlinear response," Adv. Opt. Mater. **5**, 1700753 (2017).
34. Y. Zeng, W. Hoyer, J. Liu, S. W. Koch, and J. V. Moloney, "Classical theory for second-harmonic generation from metallic nanoparticles," Phys. Rev. B **79**, 235109 (2009).
35. A. V. Krasavin, P. Ginzburg, and A. V. Zayats, "Free-electron optical nonlinearities in plasmonic nanostructures: a review of the hydrodynamic description," Laser Photon. Rev. **12**, 1700082 (2017).

36. R. Pollard, A. Murphy, W. Hendren, P. Evans, R. Atkinson, G. A. Wurtz, A. V. Zayats, and V. A. Podolskiy, "Optical nonlocalities and additional waves in epsilon-near-zero metamaterials," Phys. Rev. Lett. **102**, 127405 (2009).
37. We assume that the fields propagate in xz plane; s-polarized light has non-zero components of E_y, H_x, H_z, while the p-polarized light has components of E_x, E_z, H_y fields. We limit our study to the regime when the metamaterial is excited by a single electromagnetic wave that is either p or s polarized. The detailed investigation of more complicated excitation geometries and the analysis of tensorial properties of $\chi^{(2)}_{\alpha;\beta\gamma}$ will be the subject of future work.
38. M. Scalora, M. A. Vincenti, D. de Ceglia, and J. W. Haus, "Nonlocal and quantum-tunneling contributions to harmonic generation in nanostructures: electron-cloud-screening effects," Phys. Rev. A **90**, 013831 (2014).
39. P. Ginzburg, D. Roth, M. E. Nasir, P. Segovia, A. V. Krasavin, J. Levitt, L. M. Hirvonen, B. Wells, K. Suhling, D. Richards, V. A. Podolskiy, and A. V. Zayats, "Spontaneous emission in non-local materials," Light Sci. Appl. **6**, e16273 (2017).
40. M. A. Vincenti, D. de Ceglia, and M. Scalora, "Nonlinear dynamics in low permittivity media: the impact of losses," Opt. Express **21**, 29949–29954 (2013).
41. L. Carletti, D. Rocco, A. Locatelli, C. D. Angelis, V. F. Gili, M. Ravaro, I. Favero, G. Leo, M. Finazzi, L. Ghirardini, M. Celebrano, G. Marino, and A. V. Zayats, "Controlling second-harmonic generation at the nanoscale with monolithic AlGaAs-on-AlOx antennas," Nanotechnology **28**, 114005 (2017).

193.61.203.143 {ts '2019-08-09 08:52:46'}